ACS Sustainable Chemistry & Engineering

Research Article

pubs.acs.org/journal/ascecg

Cellulose, Chitosan and Keratin Composite Materials: Facile and Recyclable Synthesis, Conformation and Properties

Chieu D. Tran* and Tamutsiwa M. Mututuvari

Department of Chemistry, Marquette University, 535 N. 14th Street, Milwaukee, Wisconsin 53233, United States

Supporting Information

ABSTRACT: A method was developed in which cellulose (CEL) and/or chitosan (CS) were added to keratin (KER) to enable [CEL/CS+KER] composites formed to have better mechanical strength and wider utilization. Butylmethylimmidazolium chloride ([BMIm$^+$Cl$^-$]), an ionic liquid, was used as the sole solvent, and because the majority of [BMIm$^+$Cl$^-$] used (at least 88%) was recovered, the method is green and recyclable. FTIR, XRD, ^{13}C CP-MAS NMR and SEM results confirm that KER, CS and CEL remain chemically intact and distributed homogeneously in the composites. We successfully demonstrate that the widely used method based on the deconvolution of the FTIR bands of amide bonds to determine secondary structure of proteins is relatively subjective as the conformation obtained is strongly dependent on the choice of parameters selected for curve fitting. A new method, based on the partial least squares regression analysis (PLSR) of the amide bands, was developed, and proven to be objective and can provide more accurate information. Results obtained with this method agree well with those by XRD, namely they indicate that although KER retains its second structure when incorporated into the [CEL+CS] composites, it has relatively lower α-helix, higher β-turn and random form compared to that of the KER in native wool. It seems that during dissolution by [BMIm$^+$Cl$^-$], the inter- and intramolecular forces in KER were broken thereby destroying its secondary structure. During regeneration, these interactions were reestablished to reform partially the secondary structure. However, in the presence of either CEL or CS, the chains seem to prefer the extended form thereby hindering reformation of the α-helix. Consequently, the KER in these matrices may adopt structures with lower content of α-helix and higher β-sheet. As anticipated, results of tensile strength and TGA confirm that adding CEL or CS into KER substantially increase the mechanical strength and thermal stability of the [CS/CEL+KER] composites.

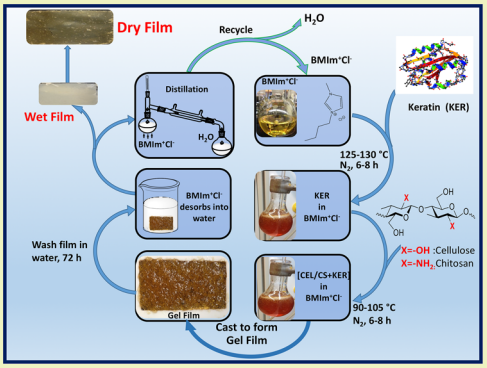

KEYWORDS: *Green chemistry, Ionic liquid, Partial least squares regression analysis, Polysaccharides, Wool*

INTRODUCTION

Nonantigenic keratin is known to possess advantages for wound care, tissue reconstruction, cell seeding and diffusion, and drug delivery as topical or implantable biomaterial.[1−5] As implantable film, sheet, or scaffold, keratin can be absorbed by surrounding tissue to provide structural integrity within the body while maintaining stability under mechanical load, and in time can break down to leave neo-tissue. Keratin is found to be characteristically abundant in cysteine residues (7−20% of the total amino acid residues).[1−5] These cysteine residues are oxidized to give inter- and intramolecular disulfide bonds, which results in three-dimensionally linked network of keratin fiber. Interestingly, in spite of its unique structure, keratin has relatively poor mechanical properties, and as a consequence, it was not possible to exploit fully unique properties of keratin for various applications.[1−5]

Polysaccharides such as cellulose (CEL) are known to have strong mechanical property,[6,7] and chitosan (CS) to have ability to stop bleeding (hemostasis), heal wounds, kill bacteria and adsorb organic and inorganic pollutants.[8−11] It is, therefore, possible that adding CEL and/or CS to KER would enhance the mechanical properties of the [CEL/CS+KER] composites so that they can be practically used for a variety of applications that hitherto were not possible. We have demonstrated recently that a simple ionic liquid, butylmethylimmidazolium chloride ([BMIm$^+$Cl$^-$]), can dissolve both CEL and CS, and by use of this [BMIm$^+$Cl$^-$] as the sole solvent, we developed a simple, GREEN and totally recyclable method to synthesize [CEL+CS] composites just by dissolution without using any chemical modifications or reactions.[12−14] The [CEL+CS] composite obtained was found to be not only biodegradable and biocompatible but also retain unique properties of its component.[12−14] Because [BMIm$^+$Cl$^-$] can also dissolve KER, it may be possible to use this IL as the sole solvent to synthesize [CEL/CS+KER] composites in a single step.

Such consideration prompted us to initiate this study that aims to improve the mechanical properties of the KER composites by adding either CEL or CS to the composites,

Received: January 13, 2016
Revised: February 6, 2016
Published: February 8, 2016

DOI: 10.1021/acssuschemeng.6b00084
ACS Sustainable Chem. Eng. 2016, 4, 1850−1861

and to demonstrate that the composites will retain unique properties of their components. In this paper, we will report results of the synthesis and spectroscopic characterization of the [CEL/CS+KER] composites. We will also report on the novel partial least squares regression (PLSR) method that we develop to determine the secondary structrue of KER in the composites.

The motivation for us to develop this PLSR method stems from the fact that results from our previous studies indicate that dissolution by and regeneration from [$BMIm^+Cl^-$] do not alter chemical structure of CEL and CS.[12−14] It is possible that the regenerated KER may also retain some of its structure as well. It is known that different from polysaccharides, which are known to have only random structure, the protein KER has secondary structure.[1−5] The secondary structure of KER in [CEL/CS +KER] composites may be modified during the synthesis. It is of particular importance to determine how much of the secondary structure (α-helix and β-sheet) is retained when it is incorporated into the [CEL+CS+KER] in composites. Such information is important because, the secondary structure of the composites strongly affects their properties including porosity, antimicrobial and antiviral activity and their ability to encapsulate and controlled release of drugs.

Circular dichroism (CD) is known to be very effective for the determination of protein secondary structure but it is effective only for solution phase[15−17] When use for solid samples, particularly for amorphous solids, it is seriously plagued by many artifacts including induced linear dispersion and linear birefringence and depolarization at grain boundaries.[16,17] Solution NMR can provide information on the location of secondary structural elements within the protein sequence.[18−20] It is, however, effective only for proteins with MW < 30K and with knowledge on chemical shifts of particular residues in the protein,[18−20] Because MWs of CEL, CS and KER are much higher than 40−70 KDa, it is not possible to use NMR for the composites. As will be demonstrated in the section below, a method based on the deconvolution of the FTIR amide I band into bands corresponding to α-helix, β-sheet and random is subjective as it is strongly dependent on choice of parameters selected for curve fitting.[21−23]

In this paper, we describe the theory of the novel PLSR method that we have developed, and report on experimental results obtained using this method to demonstrate clearly that it is more objective and provides accurate results than all other methods.

EXPERIMENTAL SECTION

Chemicals. Chitosan (MW ≈ 310−375 kDa), and microcrystalline cellulose (DP ≈ 300),[12−14] were purchased from Sigma-Aldrich (Milwaukee, WI). The degree of deacetylation of chitosan, determined by FT-IR, was found to be 84 ± 2% .[13] Raw sheep (untreated) wool, obtained from a local farm, was cleaned by Soxhlet extraction using a 1:1 (v/v) acetone/ethanol mixture at 80 ± 3 °C for 48 h. The wool was then rinsed with distilled water and dried at 100 ± 1 °C for 12 h.[2] 1-Methylimidazole and *n*-chlorobutane (Alfa Aesar, Ward Hill, MA) were distilled prior to using for synthesis of [$BMIm^+Cl^-$].[12−14]

The protein standards, used to construct a PLSR model to estimate the secondary structure of KER, included albumins (bovine serum albumin, BSA and human serum albumin, HSA); hemoglobin (horse, HEM); lysozyme (egg white, LYZ); myoglobin (horse skeletal muscle, MYO); pepsin A (porcine stomach, PEP); ribonuclease A (bovine pancrease, RNASE A); and trypsin inhibitor (soybean, SOY). Except for PEP and SOY, which were purchased from Worthington Biochemical Corporation (Lakewood, NJ), all the other protein standards were purchased from Sigma-Aldrich (St Louis, MO). All the proteins were received in lyophilized powder form and they were used without further purification.

Instruments. FTIR spectra (from 450 to 4000 cm^{-1}) were recorded on a Spectrum 100 Series FTIR spectrometer (PerkinElmer, USA) at a resolution of 2 cm^{-1} by the KBr method. Each spectrum was an average of 64 individual spectra. X-ray diffraction (XRD) measurements were taken on a Rigaku MiniFlex II diffractometer utilizing the Ni filtered Cu Kα radiation (1.540 59 Å). The voltage and current of the X-ray tube were 30 kV and 15 mA, respectively. The samples were measured within the 2θ angle range from 2.0 to 40.00. The scan rate was 50 per minute. Data processing procedures were performed with the Jade 8 program package.[24] The surface and cross-sectional morphologies of the composite films were examined under vacuum with a JEOL JSM-6510LV/LGS Scanning Electron Microscope with standard secondary electron (SEI) and backscatter electron (BEI) detectors. Prior to SEM examination, the film specimens were made conductive by applying a 20 nm gold−palladium-coating onto their surfaces using an Emitech K575x Peltier Cooled Sputter Coater (Emitech Products, TX). The tensile strength of the composite films were evaluated on an Instron 5500R tensile tester (Instron Corp., Canton, MA) equipped with a 1.0 kN load cell and operated at a crosshead speed of 5 mm min^{-1}. Each specimen had a gauge length and width of 25 mm and 10 mm, respectively. Thermogravimetric analyses (TGA) (TG 209 F1, Netzsch) of the composite films were investigated at a heating rate of 10 °C min^{-1} from 30 to 600 °C under a continuous flow of 20 mL min^{-1} nitrogen gas.

Determination of Secondary Structure of Keratin by Deconvoluting Amide I Band. Amide I band in the FTIR spectrum was deconvoluted into individual Gaussian bands using Origin Pro 9.0 software (OriginLab, USA). Each band was integrated to obtain its area. The individual bands were assigned to α-helix (1657−1650 cm^{-1}), β-sheet (1640−1612 cm^{-1}), and disordered (1697−1670 cm^{-1}) conformations.[25,26] Then, the proportional content of each band was calculated by dividing the area of the band by the total area of all the bands within the amide I region.

Determination of Secondary Structure of Keratin by Partial Least Squares Regression (PLSR) Method. Multivariate data analysis by PLS regression (PLSR) was carried out using Unscrambler X10.1 software (CAMO Inc., Oslo, Norway). A detailed treatment of this PLSR is described elsewhere.[27] Briefly, PLSR builds a linear model that relates two data matrices, the predictors (**X**) and the response (**Y**), to each other by using least-squares fitting technique. In this case, **X** contains spectra of each of the eight protein standards from 1700 to 1450 cm^{-1}; this frequency range was chosen because it was reported to contain much information about the secondary structure of proteins.[28−31] **Y** contains information about the secondary structure of the standard proteins. The model can therefore be represented by the equation:

$$\mathbf{Y} = \mathbf{XB} \quad (1)$$

where **B** contains columns of regression coefficients at each frequency. The goal is to calculate **B**, which can subsequent be used to predict the composition of the unknown. In PLSR, **B** is calculated by decomposing **X** and **Y** matrices into latent variables (principal components, PCs) which maximize covariance between **X** and **Y**. After the **B** matrix is obtained, the secondary structure can then be calculated using the relation:

$$\mathbf{Y} = \mathbf{Bx} \quad (2)$$

where **x** is the spectrum of the unknown protein sample.

The success of PLSR is determined by selecting those frequency variables that correlate well with the secondary structure motifs (i.e., α and β). The method of cross model validation (CMV) with Jack-knifing was selected for this purpose.[32,33] This model ensures variable selection without overfitting and or selecting false positive variables.[34,35] Each inner model in CMV consisted of seven proteins each time. For Jack-knifing, variables with *p*-value less than 0.05 for either α-helix or β-sheet were considered significant and, therefore, retained in the model. It is noteworthy to add that all spectra were baseline corrected and autoscaled by standard normal variate (SNV)

DOI: 10.1021/acssuschemeng.6b00084
ACS Sustainable Chem. Eng. 2016, 4, 1850−1861

Scheme 1. Procedure Used To Prepare the [CEL+CS+KER] Composite Materials

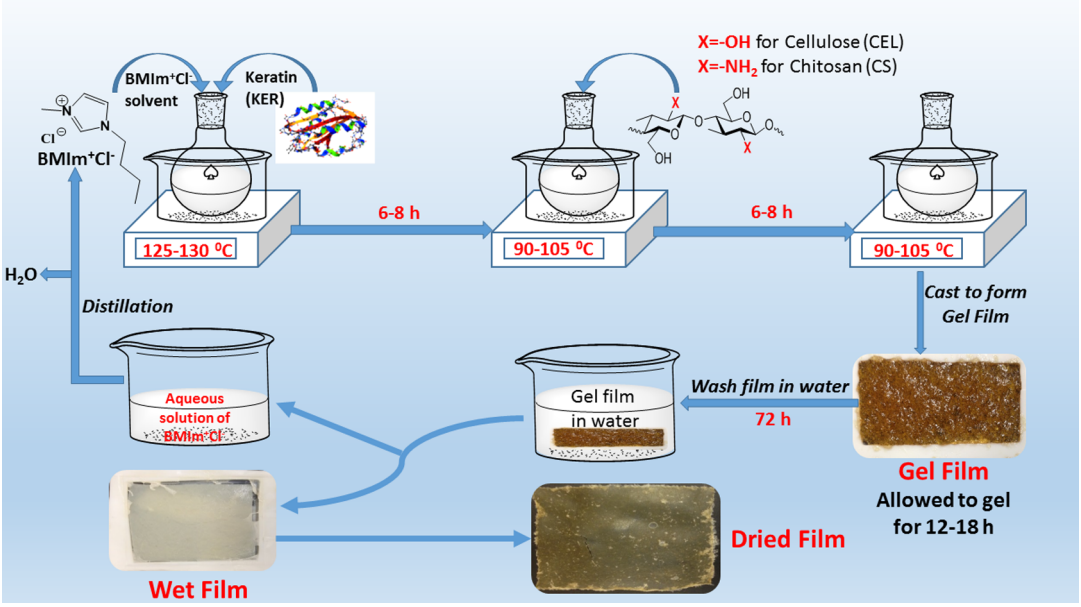

method. In addition, the data were mean centered each time before PLSR modeling. All these routines are already integrated in the Unscrambler software that was used.

The X-ray structures of the eight proteins, constituting our reference set, were taken from the Protein Data Bank (PDB).[36] The secondary structures of these proteins were evaluated using the algorithm Define Secondary Structure of Proteins (DSSP), which is integrated in the PDB program. The DSSP algorithm works by assigning secondary structure to the amino acids of a protein given the atomic resolution coordinates of the protein. Details on this method are presented elsewhere.[37] On the basis of this algorithm, eight types of secondary structure are assigned. However, in this study, only 3 groups were assigned viz α-helix, β-sheet and the remainder was assigned to an unordered group. The proteins used together with their PDB IDs and resultant secondary structures are listed in Table SI-1 of the Supporting Information.

RESULTS AND DISCUSSION

Synthesis of [CEL/CS+KER] Composites. We successfully synthesized one- (CEL/CS, and KER), two- ([CEL+KER], [CEL+CS] and three- ([CEL+CS+KER]) component composite films by using [$BMIm^+Cl^-$], an ionic liquid, to dissolve CEL, CS and KER. As shown on Scheme 1, wool dissolution required relatively higher temperature (120 °C) than that needed for either CEL or CS (90 °C). This may be due to the types of bond networks present in these biopolymers. The three-dimensional structures of CEL, CS and KER are known to be stabilized by inter- and intramolecular hydrogen bonding. In addition to this hydrogen bonding network, KER has an extensive network of disulfide (−S−S−) linkages both within and between its protein chains. It seems that this additional bond network imparts additional tightness into its structure thereby impeding the penetration of solvent molecules into its fibers. As a consequence, higher temperature is needed to dissolve the wool.

When synthesizing two- or three-component films, it was found that the order of addition of the biopolymers is very critical. For example, all KER-based composites were synthesized by first dissolving wool at 120 °C. Once dissolved, the solution temperature was reduced to 90 °C before CEL or CS was added to the KER solution. Initially, when CEL was added in 1% weight portions to the $BMIm^+Cl^-$ solution of KER, it seems that the latter enwrapped around the former, leading to the formation of small lumps of CEL. It was time-consuming and difficult to dissolve completely these lumps. To circumvent this problem, a smaller amount (ca. 0.5% weight portion) of CEL was subsequently added. For the synthesis of [CEL+CS] composites, CEL was dissolved first before adding CS. If CS is dissolved first, it would form relatively high viscous solution which would make it difficult to dissolve completely CEL, which may produce inhomogeneous composite material. Using this procedure, [$BMIm^+Cl^-$] solution of CEL, CS and KER containing up to total concentration of 6 wt % (relative to IL) with various compositions and concentrations were prepared.

The resulted solution was cast onto PTFE molds with desired thickness on Mylar films to produce thin films of 2- and 3-component films with different compositions and concentrations of CEL, CS and KER. They were then allowed to undergo gelation at room temperature to yield gel films. Because [$BMIm^+Cl^-$] is known to exhibit some toxicity to living organisms[12−14] it was removed from the composites by washing the gel films with water for at least 3 days. The washing water was replaced with fresh water 3 times on the first day and 2 times on day 2 and day 3. Concentration of [$BMIm^+Cl^-$] in the wash water was determined by UV−visible absorption at 209 nm. On the basis of the absorptivity of [$BMIm^+Cl^-$], at the end of the washing, if any of the IL was present in the wash water, it was less than 56 pg/1 mL of water. Because no [$BMIm^+Cl^-$] was detected on the composite films by FTIR, NIR and UV, it is very likely that the IL was completely removed from the films by washing them with water. Even if any of it ever remained, it would be of less than 56 pg/1g of composite film. The [$BMIm^+Cl^-$] in wash water was recovered by distilling the wash solution, and then dried under vacuum at 70 °C overnight before being reused. Finally, dried films were obtained when the wet films were allowed to dry at room temperature in a humidity-controlled chamber.

Spectroscopic Characterization. *Fourier Transform Infrared (FTIR).* FTIR was used to (1) confirm that CEL, CS

DOI: 10.1021/acssuschemeng.6b00084
ACS Sustainable Chem. Eng. 2016, 4, 1850−1861

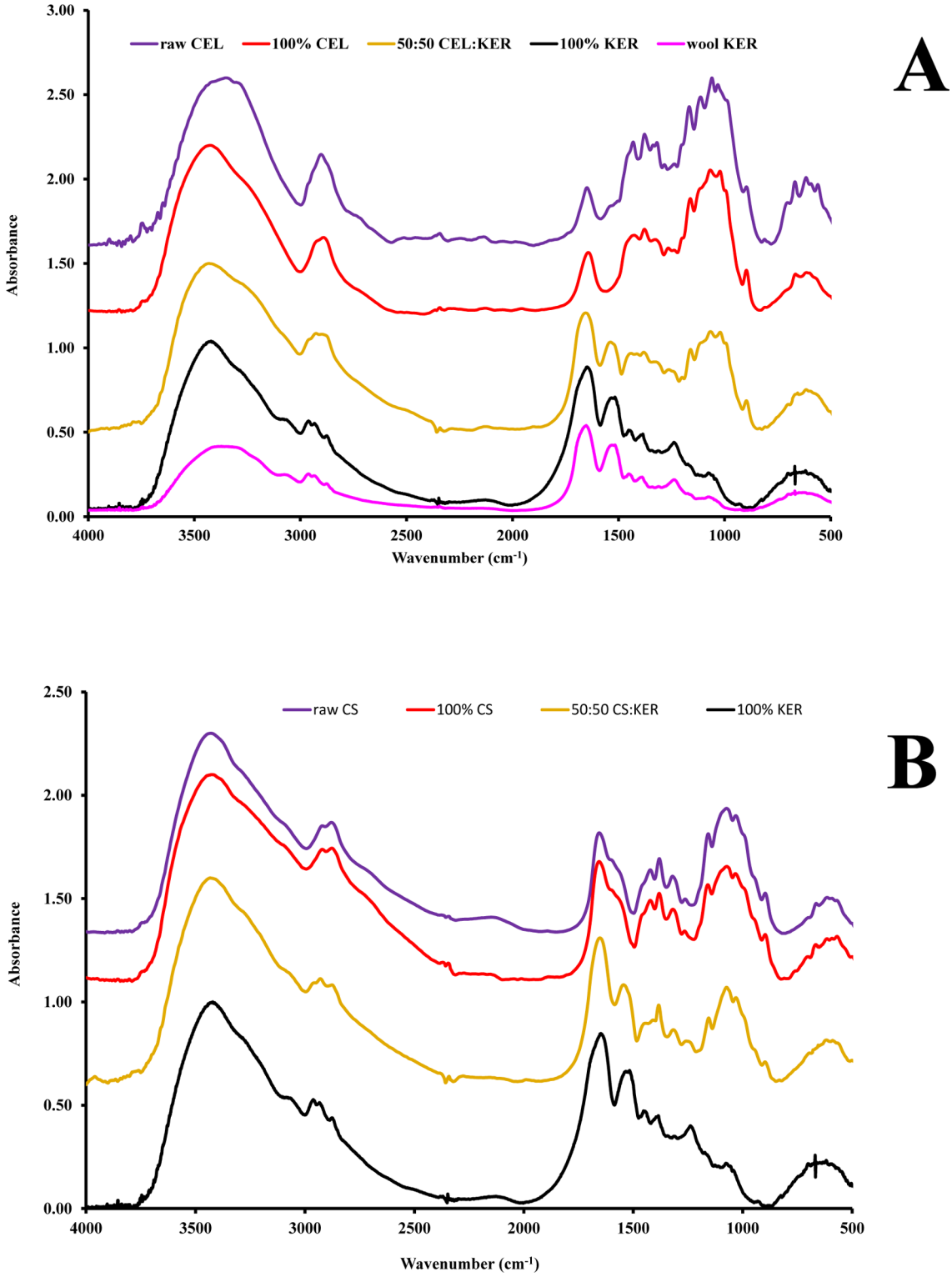

Figure 1. FTIR spectra of different composition of (A) [CEL+KER] and (B) [CS+KER] composites.

and KER were not chemically altered by dissolution with and regeneration from ionic liquids; and (2) determine the secondary structure of keratin the [CEL+CS+KER] composite films.

FTIR spectra of wool, shown as the pink curve in Figure 1A, exhibited characteristic bands that can be assigned to the vibrational modes of peptide bonds in proteins. For examples; the bands at 1700−1600 and 1550 cm^{-1} are due to amide C═O stretch (amide I) and C—N stretch (amide II) vibrations, respectively.[38] In addition, the 3280 cm^{-1} band can be assigned to N—H stretch vibration (amide A) whereas a band at 1300−1200 cm^{-1} is due to the in-phase combination of the N—H bending and the C—N stretch vibrations (amide III). This finding is expected because wool contains more than 95% of keratin protein.[39] It is noteworthy to add that the FTIR spectrum of wool does not have any band at 1745 cm^{-1}, which

DOI: 10.1021/acssuschemeng.6b00084
ACS Sustainable Chem. Eng. 2016, 4, 1850−1861

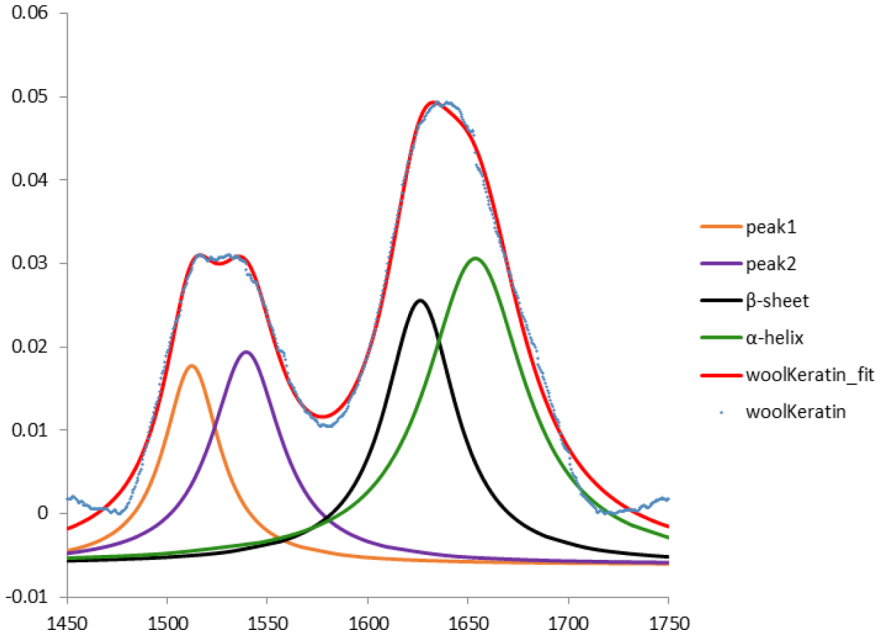

Figure 2. Deconvolution of amide band 1 band of wool; dashed-line blue curve, wool; red curve, best fit.

is known to be due to lipid ester carbonyl vibrations.[40] It seems, therefore, that the Soxhlet extraction effectively removed all residual lipids from wool. Interestingly, upon regenerating KER film from the wool, no new IR signatures were detected in the FTIR spectrum of the former (compare pink spectrum for wool to the black spectrum for 100% KER). This suggests that dissolution by and regeneration of KER from $BMIm^+Cl^-$ do not produce any chemical alteration on the chemical structure of KER. It is, therefore, reasonable to expect that the properties of wool may remain intact in the regenerated KER film.

The FTIR spectra of [CEL+KER] and [CS+KER] composites with different compositions are presented in Figure 1A and B, respectively. As expected, the spectra of these composite films exhibit bands characteristic of their respective components. Furthermore, the magnitude of these bands seems to correlate well with concentration of corresponding component in the film. For example; the band between 1200 and 900 cm^{-1} (due to sugar ring deformations) increased in relative intensity concomitantly with the relative concentration of CEL in the [CEL+KER] composite films (Figure 1A). On the other hand, the intensity of the amide I and amide II bands increased with the increase in the relative concentration of KER in the same composite films. A similar behavior was also observed for [CS+KER] composite films (Figure 1B). It is noteworthy to add that, in all composite films ([CEL+KER], [CS+KER] and [CEL+KER+CS]), no new bands are found in their FTIR spectra; i.e., the spectra of the composites are a superposition of the spectra of the corresponding individual components. This, as noted earlier, further confirms that no chemical alterations occurred during the synthesis of these composites, and that the composites obtained are expected to retain the properties of their components.

Analysis of Secondary Structure of Keratin and its Composites. As stated above, the main chemical framework of KER was maintained during the regeneration process. It is, however, possible that its secondary structure was modified during the process. Such changes may adversely affect the properties of KER. It is, therefore, essential to determine the secondary structure of regenerated KER.

As described in the Introduction, methods such as circular dichroism (CD) and NMR are not suited for the [CEL/CS +KER] composites because in addition to being amorphous, the molecular weight of the composites is too high for the NMR method to be effective.

The FTIR method is based on the deconvolution of the FTIR amide I band into underlying bands that are assigned to α-helix, β-sheet and random form of a protein. Shown in Figure 2 are results obtained by deconvoluting the amide band of the wool keratin from 1450 to 1750 cm^{-1} into three Gaussian bands that can then be assigned to α-helix, β-sheet and random form. As illustrated, the calculated spectrum (red curve) agrees well with actual spectrum (blue dashed-line curve). Calculated concentrations of α-helix, β-sheet and random form are listed in Table 1. For reference, results for calculation made by changing the amide spectrum region by 1 or 2 cm^{-1} in either directions are also listed in the table. It is evidently clear that the results are very sensitive to the spectrum region selected for calculation. For example, by changing the spectrum region by

Table 1. Secondary Structure of Wool, Regenerated KER and Its Composites with CEL and CS Calculated by Deconvolution of FTIR Spectra

substance	spectrum range, cm^{-1}	α-helix (%)	β-sheet (%)	random coil
wool, this work	1450−1750	45.4	20.6	34.1
wool, this work	1451−1751	52.2	13.2	33.6
wool, this work	1452−1752	51.9	13.9	34.2
wool, this work	1449−1749	54.1	15.3	30.6
wool, this work	1448−1748	54.7	15.7	29.6
wool, ref 1	1450−1750	34	25	
wool, ref 2	1580−1740	47	33	19
wool, ref 3	1450−1750	58.2	37.9	3.9
100% KER	1450−1750	54.4	7.9	37.8
100% KER	1451−1751	57.4	6.0	36.6
100% KER	1452−1752	58.9	6.7	34.4
100% KER	1449−1749	59.8	7.4	32.8
100% KER	1448−1748	61.1	8.6	30.3

DOI: 10.1021/acssuschemeng.6b00084
ACS Sustainable Chem. Eng. 2016, 4, 1850−1861

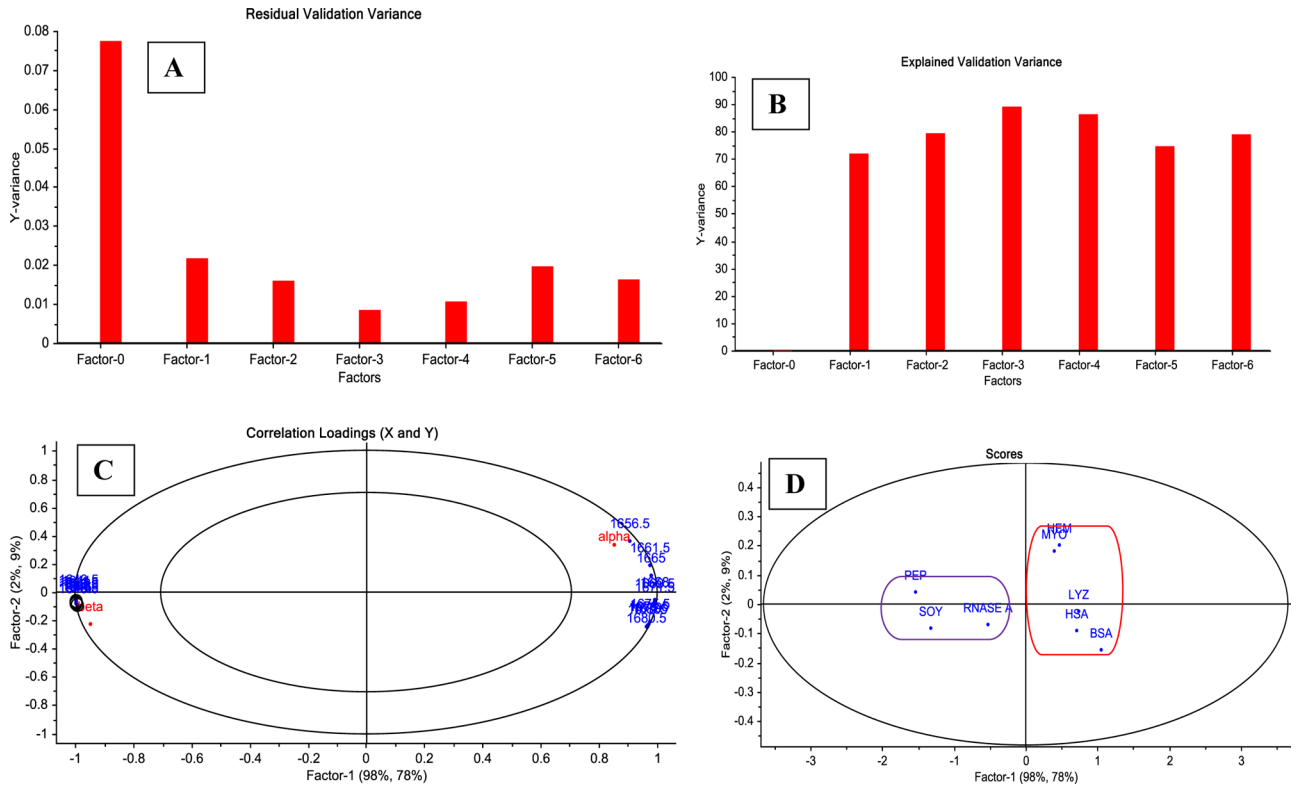

Figure 3. Plot of (A) residual validation variance: (A) explained validation variance, (B, C) scores plot, and (D) correlation loadings for *X*-variables used to build the final calibration model.

only 1 cm^{-1}, i.e., from 1450 to 1750 cm^{-1} to 1451−1751 cm^{-1}, the α-helix content of wool keratin increases from 45.4% to 52.2% or 15% change whereas the content of β-turn decreases from 20.6% to 14.2% or 31% change. Similarly, the content of α-helix and β-sheet for regenerated KER also increases by 5.5% and decreases by 23.4%, respectively by increasing the spectrum region used in calculation by only 1 cm^{-1}. Change of similar magnitude was also observed when the calculated spectrum region was decrease by 1 cm^{-1}, i.e., from 1450 to 1750 cm^{-1} to 1449−1749 cm^{-1}

It is, thus, clear that the deconvolution method is subjective, as the conformation obtained is strongly dependent on the choice of parameters selected for curve fitting. As a consequence, our efforts were subsequently concentrated on developing a new method that is more objective so that the conformation results obtained would be more accurate and reliable. Such considerations prompted us to explore the use of the partial least squares regression (PLSR) method for this purpose. In this method, only two structural motifs, α-helix and β-sheet, were modeled in the calculation even though the structure of proteins is known to be composed of varying proportions of these two motifs and other motifs (random coil or unordered). This is because the FTIR bands corresponding to α-helix and β-sheet are known to be more defined than the spectra linked to the random coil. Furthermore, the spectra linked to random coil vary from protein to protein making it difficult to model accurately this motif. Therefore, the remaining fraction, that is the fraction not attributed to any of α-helix and β-sheet, was assumed to be associated with random structures.

The first stage is to select a set of predictor (X) variables that correlate well with the response (Y) variables studied. In this case, we used cross model validation (CMV) with Jack-knifing to estimate p-values for each X-variable as described above.[41] Only X-variables with p-values less than 0.05 on either α or β were retained in the model. The number of times each X-variable that was found to be significant in the eight inner models of CMV was then recorded, and the results are shown as Figure SI-1 in the Supporting Information. A set with variables exhibiting the highest frequency (that is eight in the current case) was used to build another model. To this set was added, a set that exhibits the next highest frequency (that is seven). This was continued until all the X-variables with frequency of at least one were used to construct the PLS model. Then, the quality of these models were evaluated based on root-mean-square error (RMSE), coefficient of determination (R^2) and the optimal number of latent variables (LVs). The model with the lowest RMSE, highest R^2 and optimal number of LVs was selected for use in predicting the secondary structure of KER in wool, regenerated KER, CS:KER and CEL:KER composites. The best model that fulfilled these criteria consisted of X-variables with a frequency of significance of at least seven.

Figure 3 summarizes the PLSR results for the chosen PLSR model. The residual validation variance tend to decrease with more factors being incorporated into the model (Figure 3A). This is because incorporating more factors into the model produces more systematic variations. However, the residual validation variance started increasing beyond three factors, which seems to indicate that the model is now incorporating noise. Because only factors describing systematic variation should be used in the model, only three factors were used to build the calibration model for predictions of unknowns. It was also necessary to check the relative amount of variation explained when this optimum number of factors was used. Figure 3B shows that the three factors accounted for 89%

DOI: 10.1021/acssuschemeng.6b00084
ACS Sustainable Chem. Eng. 2016, 4, 1850−1861

variance, which is a high value. The scores plot (Figure 3C) shows that PC1 is able to separate the protein standards based on their α-helix and β-sheet composition. Along this PC, protein standards with more than 0.3 α-helix and at most 0.1 β-sheet (i.e., MYO, HEM, HAS, BSA, LYZ) group together on the right side (within the red box) whereas those standards with less than 0.2 α-helix and more than 0.3 β-sheet (RNASE A, SOY, PEP) group together on the left side (within the purple box). These differences are further confirmed when the correlation loadings plot was considered (Figure 3D). Along PC1, the α-variable tends to appear on the right-hand side whereas the β-variable appears on the opposite side. By comparing this correlation loadings plot with the scores plot, it becomes apparent that the α-variable is positively correlated with proteins containing more α-helix. Similarly, the β-variable is positively correlated with proteins containing more β-sheet. In addition, the correlation loadings shows the correlation between the Y-variables (α and β) and the X-variables (frequency). As expected, the α-helix is positively correlated to the variable 1656.5 cm^{-1}, which is consistent with the previous findings.[17,19,22,42] On the other hand, the β-sheet is positively correlated to variables 1642.0−1640.5 cm^{-1}. Plots of predicted versus reference for α-helix and β-sheet components are presented in Figures SI-2A,B, respectively. Cross validation for α-helix gave RMSECV and R^2 of 0.118 and 0.874, respectively whereas 0.053 and 0.934 were obtained for the β-sheet. The results seems to indicate that the model predicts β-sheet content relatively more accurately than α-helix content.

The model was then applied to predict the α-helix and β-sheet contents of KER in wool, regenerated KER, CS:KER and CEL:KER composites. Results obtained are listed in Table 2.

Table 2. Secondary Structure of Wool, Regenerated KER and Its Composites with CEL and CS Calculated by PLSR Method

	α-helix (%)	β-sheet (%)
wool	33 ± 2	18.1 ± 0.4
KER100	31 ± 8	21 ± 3
25:75 CS:KER	18 ± 4	31 ± 4
25:75 CEL:KER	32 ± 9	25 ± 4

Wool was found to contain (33 ± 2)% α-helix and (18.1 ± 0.4)% β-sheet. These results corroborate the previous findings that sheep wool contains more α-helix than β-sheet. Upon dissolving in IL and regenerating from water, KER was found to contain (31 ± 8)% α-helix and (21 ± 3)% β-sheet. These results suggest that the regenerated KER adopts a similar conformation as that of wool but with relatively lower amount of α-helix and higher β-sheet structure. Using the FTIR method based on the deconvolution of the amide band, other groups also found similar results, namely, regenerating KER leads to lower content of α-helix and higher β-sheet structure.[44−47] Subsequently, efforts were made to predict the secondary structure of KER in the CS:KER and CEL:KER composites. It is noted that the FTIR spectra of CEL and CS possess interfering bands in the amide I region. For examples, the spectrum of CEL exhibits an O−H band at 1640 cm^{-1}. Chitosan, being partially deacetylated (84 ± 2% degree of deacetylation), contains residual amide bonds, which is similar to the amide I bands. As a consequence, it is relatively more difficult to predict the secondary structure of KER composites containing either CEL or CS. However, it is expected that the interference by CS and CEL may be smaller when KER is present in relatively higher concentration. Accordingly, prediction was performed for composites containing 75% KER, namely, the 25:75 CS:KER and 25:75 CEL:KER. As shown in Table 2, the 25:75 CS:KER was found to contain (18 ± 4)% α-helix and (31 ± 4)% β-sheet whereas its CEL:KER counterpart contains (32 ± 9)% α-helix and (25 ± 4)% β-sheet. These results seem to indicate that the polysaccharides tend to stabilize more β-sheet- than α-helix-conformation. These results may be explained by considering the whole process of dissolution and regeneration. During dissolution, the inter- and intramolecular forces in KER are broken, thereby destroying its secondary structure but maintaining its primary structure. During gelation, regeneration from water and drying, these interactions are re-established, thereby reforming some of the same secondary structure as in wool. However, in the presence of the polysaccharides (either CEL or CS), the chains seem to prefer the extended form, thereby hindering reformation of the α-helix. Consequently, the KER in these composites adopts structures with relatively lower α-helix content and higher β-sheet content.

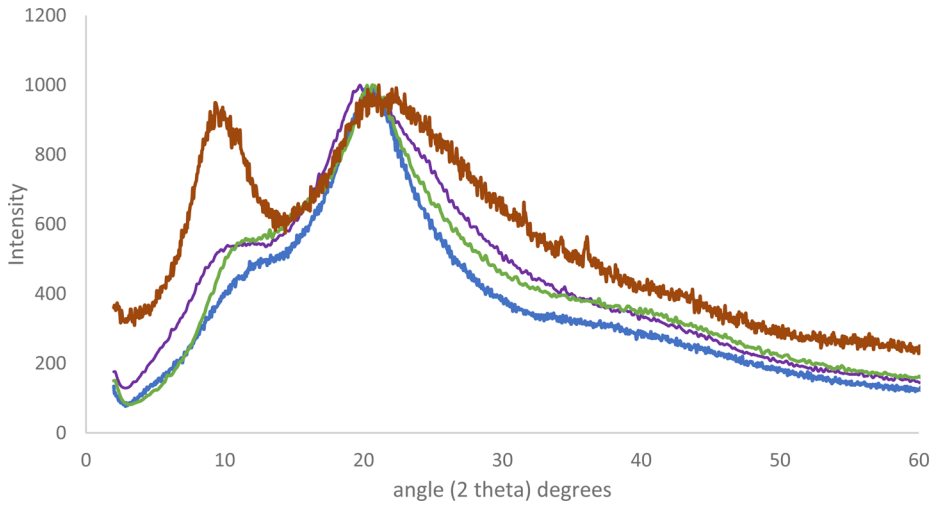

Figure 4. X-ray diffraction spectra of wool (red), regenerated KER (purple), 25:75 CS:KER (green) and 25:75 CEL:KER (blue) composite.

DOI: 10.1021/acssuschemeng.6b00084
ACS Sustainable Chem. Eng. 2016, 4, 1850−1861

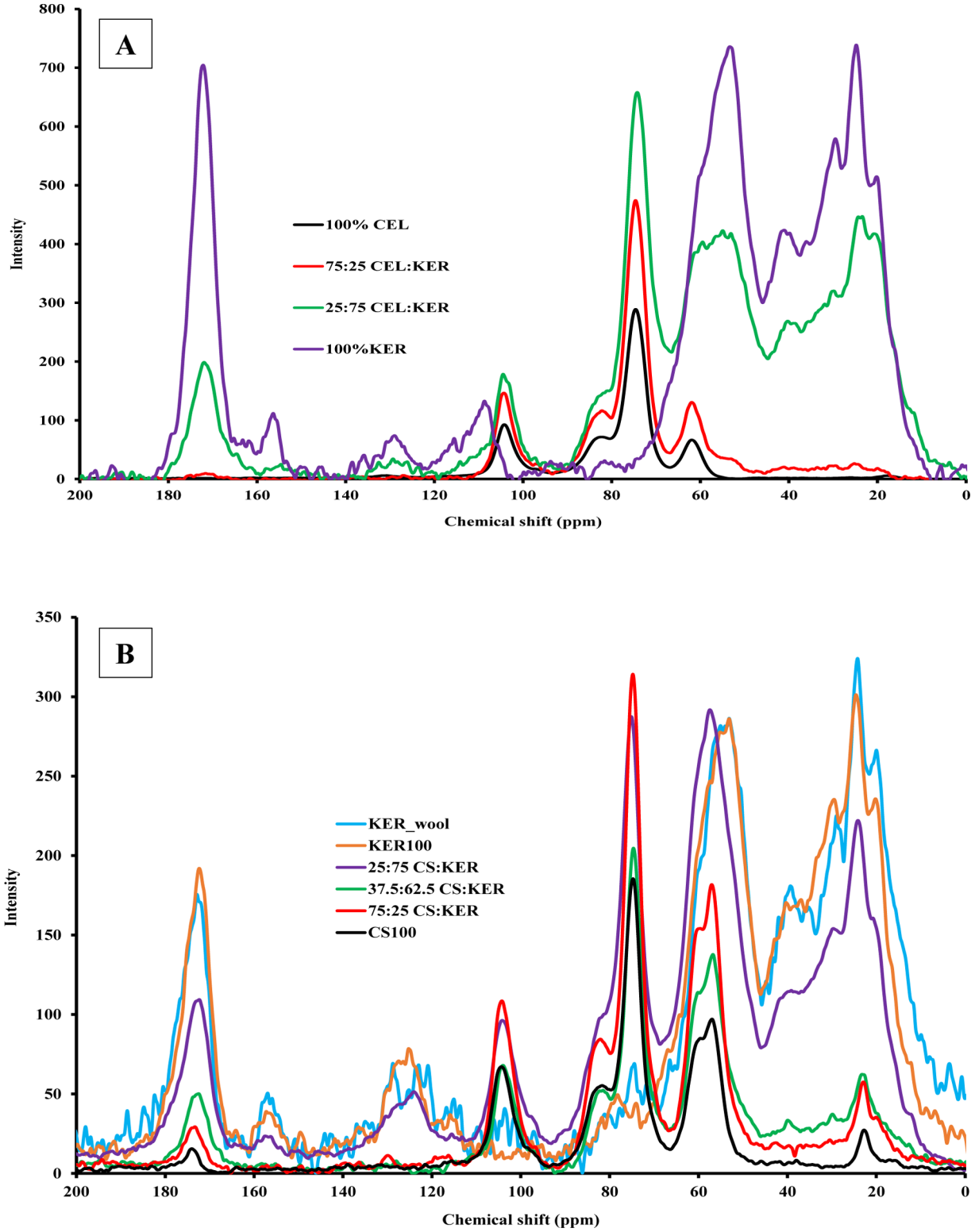

Figure 5. ^{13}C CP-MAS NMR spectra of (A) [CEL+KER] and (B) [CS+KER] composites.

Powder X-ray Diffraction (XRD). Figure 4 shows XRD spectra for wool, regenerated KER (100% KER), 25:75 CS:KER and 25:75 CEL:KER films. Wool (red curve) exhibits two bands at 2θ of about 9° and 20°. The first and the second band can be attributed to the α-helix and β-sheet structure, respectively.[46,47] The fact that the band at ~20° for the regenerated KER (purple curve) has the same intensity as that of the wool, but at ~9° it has only a broad shoulder instead of a pronounced band as in wool seems to indicate that regenerated KER has relatively lower α-helix contain and higher β-sheet, β-turn and random structure than wool. Similarly, the structure of two KER composites (25:75 CS:KER and 25:75 CEL:KER (green and blue curve)) is more similar to regenerated KER than wool, namely, relatively lower α-helix and higher β-sheet,

DOI: 10.1021/acssuschemeng.6b00084
ACS Sustainable Chem. Eng. 2016, 4, 1850−1861

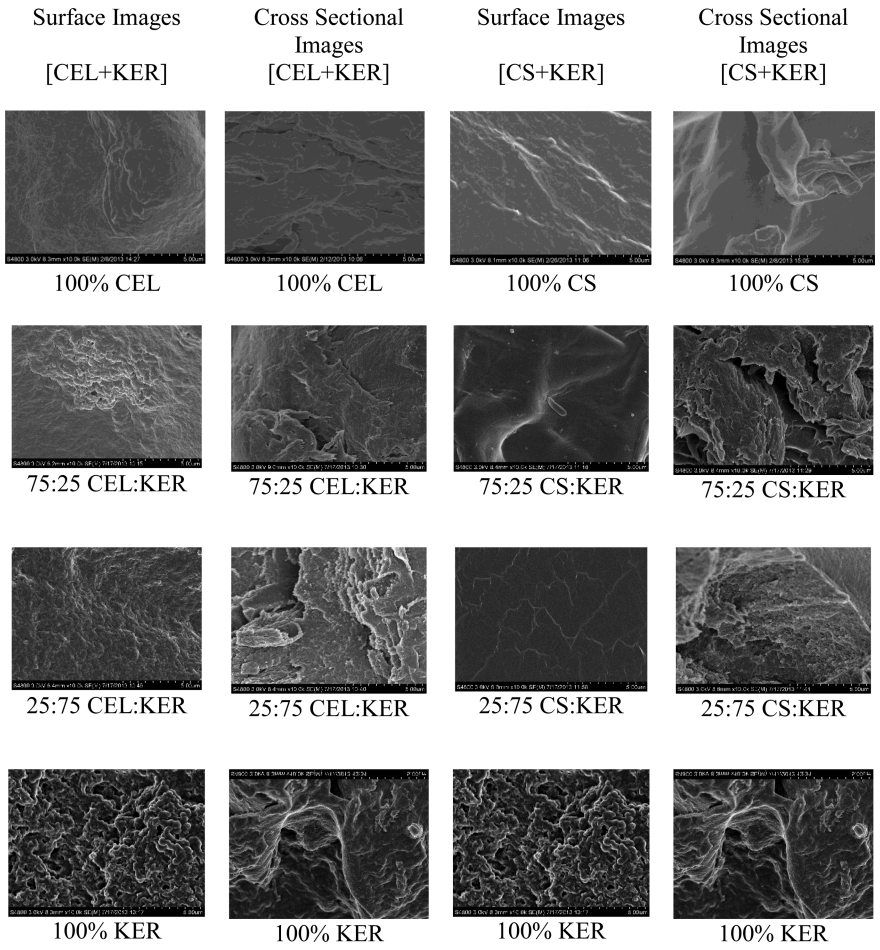

Figure 6. Surface SEM images (first and third columns) and cross-sectional images (second and fourth columns) of [CEL+KER] (first two columns on the left-hand side) and [CS+KER] (last two columns on the right-hand side).

β-turn and random structure. These results are in agreement with those presented above based on FTIR.

^{13}C Solid State-Cross-Polarization-Magic Angle Spinning (CP-MAS) NMR Spectroscopy. ^{13}C CP MAS NMR technique was used to characterize further the composites. For wool (blue spectrum in Figure 5B), the bands appearing in the ranges 172−180 ppm, 115−158 ppm, 45−65 ppm and 10−40 ppm can be assigned to carbonyl, aromatic carbons, C^{α} methane and side chain aliphatic carbon atoms, respectively.[48,49] As shown as the orange spectrum in the figure, the regenerated KER has virtually the same spectrum as that of the wool, which again confirms that no chemical alteration occur during the dissolution of wool by IL and regenerating from water. The spectrum for 100% CEL film (black spectrum in Figure 5A) contains all the bands assignable to each carbon atom of its glucose units. Specifically, the peaks appeared at 61.9 ppm (C-6), 74.6 ppm (C-3 and C-5), 83.2 ppm (C-4), 104.2 ppm (C-1). As expected, spectrum of the 25:75 CEL:KER composite (green spectrum) contains bands assignable to both CEL or KER. Similarly, the spectra of 25:75 CS:KER and 37.5:62.5 CS:KER composites contain bands corresponding to both CS and KER (Figure 5B).

Scanning Electron Microscopy (SEM). Figure 6 shows SEM images of the surfaces and cross sections of [CEL/CS+KER] composite films. Although images for 100% CS and 100% CEL surfaces exhibit smooth and homogeneous morphologies without any pores, the images of 100% KER exhibit a rough and porous structure with a three-dimensional interconnection throughout the film surface. This porous structure seems to reflect the physical properties of KER films. For example, the brittleness of 100% KER film may be partly attributed to this porous microstructure. To improve the mechanical properties of KER while harnessing its controlled drug-release properties, KER was blended with either CEL or CS. As can be seen, incorporation of the polysaccharides (CEL and CS) into the KER matrix lead to significant changes in the microstructures of the resultant composite films. However, the microstructures of these composite films are noticeably different. Although incorporation of CS in the KER matrix results in composite films that present smooth and homogeneous surfaces with no evidence for phase separation, incorporation of CEL results in somewhat rough surfaces. This suggests that KER is more compatible with CS than it is with CEL. This is so despite the similarity in the chemical structures of CEL and CS; the only difference in their chemical structures is that CS has an amine group at C-2 whereas CEL has a hydroxyl group. These results seem to indicate that [CS+KER] is more densely packed than [CEL+KER].

Mechanical Properties. Although KER has been shown to induce controlled release of drugs,[50] its poor mechanical properties continue to restrict its potential applications. For example, as previously reported and also observed in this study,[50] regenerated KER film was found to be too brittle to be reasonably used in any application. Because CEL is known to

DOI: 10.1021/acssuschemeng.6b00084
ACS Sustainable Chem. Eng. 2016, 4, 1850−1861

possess superior mechanical strength, it is possible enhance the mechanical property of KER-based composite by adding CEL or other polysaccharides such as CS into it. Accordingly, [KER +CEL] and [KER+CS] composites with different concentrations were prepared, and their tensile strength was measured. Figure 7 plots tensile strength of [CEL+KER] and [CS+KER]

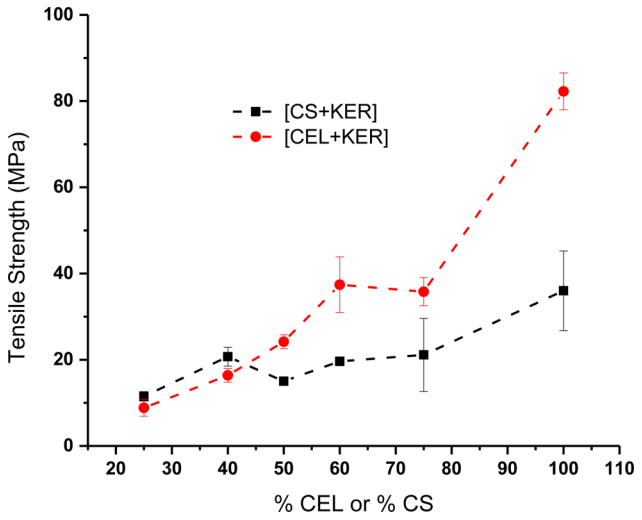

Figure 7. Plots of tensile strength as a function of %CEL in [CEL +KER] composites (red curve) and %CS in [CS+KER] composites (black curve).

composites as a function of cellulose and chitosan content. As illustrated, the tensile strength of [CEL+KER] composites was found to increase concomitantly with the content of CEL. For example, the tensile strength of [CEL+KER] increased by at least 4× when CEL loading was increased from 25% to 75%. This behavior has also been reported elsewhere when CEL was used as a reinforcement in other composites.[51] It is worth noting that [CEL+KER] composite films were much weaker than [CS+CEL].[52] For example, [CEL+KER] and [CEL+CS] containing 75% and 71% CEL had tensile strengths 36 ± 3 MPa and 52 MPa, respectively. This could be attributed to the fact that CEL structure is more similar to that of CS than KER structure. Therefore, much stronger interactions are established between CEL and CS than between CEL and KER. Although CS also leads to an increase in the tensile strength of [CS +KER], its effect is noticeably weaker than that of CEL of comparable loading. For example, [CEL+KER] and [CS+KER] had tensile strength values of 37 ± 6 MPa and 20 ± 1 MPa, respectively for a 40% KER loading. Similar results were also found for 100% CS and 100% CEL, namely the tensile strengths of 100% CS is only 36 ± 9 MPa, whereas that of 100% CEL is 82 ± 4 MPa. The fact that CS has relatively inferior mechanical strength to CEL may be explained by the differences in the structure of CS and CEL. It is a well-known fact that the strong inter- and intramolecular hydrogen bond network in CEL enables it to adopt a strong and very dense structure thereby giving it strong mechanical strenght. Compared to the hydroxy group, the amino group can only form relatively weaker hydrogen bond. The hydrogen bond network in CS is, therefore, not as extensive as in CEL, and its interior is less dense than CEL. As a consequence, CS has relatively weaker mechanical strength than CEL.

Thermal Physical Properties of [CEL/CS+KER] Composite Films. Subsequently, the thermal gravimetric analysis (TGA) was used to determine the effect of each component on the thermal properties of the resultant composite film. Effect of dissolution by IL on the thermal properties of the composites was also investigation. The comparison were achieved by using onset decomposition temperature as a surrogate measure of the thermal stability of a component. It is probable that the dissolution process could reduce the thermal stability of the biopolymers. This possibility was investigated by comparing the onset decomposition temperature of unprocessed biopolymers with corresponding regenerated films. TGA curves of wool, CEL powder, CS powder, regenerated KER, regenerated CEL (i.e., 100% CEL), regenerated CS (100%CS), and CEL:KER and CS:KER composites with different compositions are shown in Figure SI-3. Also shown in the figure are derivatives of the TGA curves of these composites from which the onset decomposition temperatures of these composites were determined. It was found that the onset decomposition temperature for KER decreased by 0.5% (i.e., from 246.8 to 245.5 °C) when regenerated from IL. Similarly, the onset decomposition temperature for CS powder decreased by 2% (from 269.9 to 264.2 °C) whereas that of the CEL powder is by 1.26% (from 318.4 to 314.0 °C). Because these changes are small and within experimental errors, the regeneration from IL leads to only very minor changes, if any, in the structure and thermal property of the biopolymers. These results seem to indicate that it is possible to use the TGA technique to determine the effect of adding one biopolymer to another. Figure 8 plots onset decomposition temperature of [CS+KER]

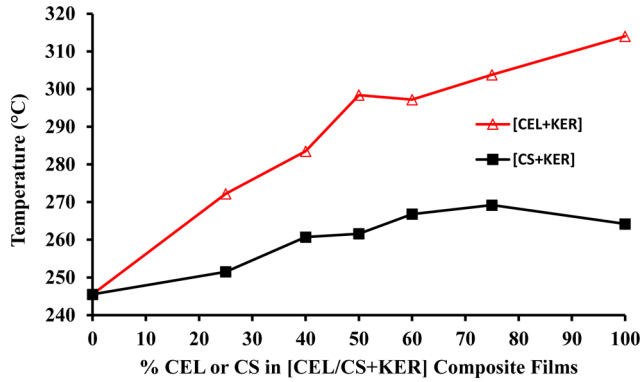

Figure 8. Plots of onset decomposition temperatures for [CEL+KER] composites (red curve with open triangles) and [CS+KER] composites (black curve with filled squares).

and [CEL+KER] composites as a function of concentration of CS or CEL. As illustrated, 100% KER was the least thermally stable followed by CS and then CEL. As expected, composites of KER with each of the polysaccharides show an improvement in the thermal stability as the proportional content of either CEL or CS increases. Therefore, by judiciously selecting the composition of CEL, CS and KER, the thermal properties of the [CEL/CS+KER] composites can be appropriately adjusted.

CONCLUSIONS

In summary, we have shown that KER and its composites with CEL and/or CS were successfully and readily synthesized in a one-step process in which [$BMIm^+Cl^-$], an ionic liquid, was used as the sole solvent for dissolution of the wool and polysaccharides. Because the majority of [$BMIm^+Cl^-$] used (at least 88%) was recovered, the method is green and recyclable.

DOI: 10.1021/acssuschemeng.6b00084
ACS Sustainable Chem. Eng. 2016, 4, 1850−1861

Results of FTIR, XRD, ^{13}C CP MAS NMR and SEM confirm that KER, CS and CEL remain chemically intact and homogeneously distributed in the regenerated composites. We have shown that the widely used method based on the deconvolution of the FTIR bands of amide bonds to determine secondary structure of proteins is relatively subjective as the conformation obtained is strongly dependent on the choice of parameters selected for curve fitting. A new method, based on the partial least squares regression (PLSR) analysis of the FTIR amide bands, was developed and proven to be objective and can provide relatively more accurate information. Results obtained with this PLSR method agree well with those deduced by XRD. Both of these methods indicate that the secondary structure of the regenerated KER and [CEL/CS+KER] composites have relatively lower α-helix, higher β-turn and random form compared to that of the KER in native wool. It seems that during dissolution by $BMIm^+Cl^-$, the inter- and intramolecular forces in KER are broken thereby destroying its secondary structure but maintaining its primary structure. During gelation, regeneration from water and drying, these interactions are reestablished thereby reforming some of the same secondary structure as in wool. However, in the presence of the polysaccharides (either CEL or CS), the chains seem to prefer the extended form thereby hindering reformation of the α-helix. Consequently, the KER in these matrices adopts structures with lower content of α-helix and higher β-sheet. As anticipated, results of tensile strength and TGA confirm that adding CEL or CS into KER substantially increase the mechanical strength and thermal stability of the [CS/CEL+KER] composites. Because KER, CS and CEL remain chemically intact in the composites, it is expected that the composites will retain unique properties of their components. The improved mechanical and thermal physical properties of the KER composites make it possible to exploit fully its properties in various applications including antibacterial activity and drug delivery. These are the subject of our subsequent publications.

■ ASSOCIATED CONTENT

Supporting Information

The Supporting Information is available free of charge on the ACS Publications website at DOI: 10.1021/acssuschemeng.6b00084.

(PDF)

■ AUTHOR INFORMATION

Corresponding Author

*Chieu D. Tran. Tel.: (414) 288 5428. Email: chieu.tran@marquette.edu.

Notes

The authors declare no competing financial interest.

■ ACKNOWLEDGMENTS

The authors are grateful to Dr. Raymond Fournelle for his competent assistance to measure SEM. Research reported in this publication was supported by the National Institute of General Medical Sciences of the National Institutes of Health under Award number R15GM099033.

■ REFERENCES

(1) Vasconcelos, A.; Cavaco-Paulo, A. The use of keratin in biomedical applications. *Curr. Drug Targets* **2013**, *14*, 612−619.

(2) Cui, L.; Gong, J.; Fan, X.; Wang, P.; Wang, Q.; Qiu, Y. Transglutaminase-modified wool keratin film and its potential application in tissue engineering. *Eng. Life Sci.* **2013**, *13*, 149−155.

(3) Xu, S.; Sang, L.; Zhang, Y.; Wang, X.; Li, X. Biological evaluation of human hair keratin scaffolds for skin wound repair and regeneration. *Mater. Sci. Eng., C* **2013**, *33*, 648−655.

(4) de Guzman, R. C.; Merrill, M. R.; Richter, J. R.; Hamzi, R. I.; Greengauz-Roberts, O. K.; Van Dyke, M. E. Mechanical and biological properties of keratose biomaterials. *Biomaterials* **2011**, *32*, 8205−8217.

(5) Rouse, J. G.; Van Dyke, S. M. A review of keratin-based biomaterials for biomedical applications. *Materials* **2010**, *3*, 999−1014.

(6) Augustine, A. V.;. Hudson, A. B.; Cuculo, J. A. Direct solvents for cellulose. In *Cellulose Sources and Exploitation*; Kennedy, John, F.; Phillips, Glyn, O.; Williams, Peter, A., Eds.; Ellis Horwood: New York, 1990; pp 59−65.

(7) Dawsey, T. R. Applications and limitations of lithium chloride/N,N-dimethylacetamide in the homogeneous derivatization of cellulose. In *Cellulosic Polymers, Blends and Composites*; Gilbert, Richard, D., Ed.; Carl Hanser Verlag: New York, 1994; pp 157−171.

(8) Burkatovskaya, M.; Tegos, G. P.; Swietlik, E.; Demidova, T. N.; P. Castano, A. P.; Hamblin, M. R. Use of chitosan bandage to prevent fatal infections developing from highly contaminated wounds in mice. *Biomaterials* **2006**, *27*, 4157−4164.

(9) Kiyozumi, T.; Kanatani, Y.; Ishihara, M.; Saitoh, D.; Shimizu, J.; Yura, H.; Suzuki, S.; Okada, Y.; Kikuchi, M. Medium (DMEM/F12)-containing chitosan hydrogel as adhesive and dressing in autologous skin grafts and accelerator in the healing process. *J. Biomed. Mater. Res., Part B* **2006**, *79B*, 129−136.

(10) Jain, D.; Banerjee, R. Comparison of ciprofloxacin hydrochloride-loaded protein, lipid, and chitosan nanoparticles for drug delivery. *J. Biomed. Mater. Res., Part B* **2008**, *86B*, 105−112.

(11) Naficy, S.; Razal, J. M.; Spinks, G. M.; Wallace, G. G. Modulated release of dexamethasone from chitosan-carbon nanotube films. *Sens. Actuators, A* **2009**, *155*, 120−124.

(12) Tran, C. D.; Duri, S.; Harkins, A. L. Recyclable synthesis, characterization, and antimicrobial activity of chitosan-based polysaccharide composite materials. *J. Biomed. Mater. Res., Part A* **2013**, *101A*, 2248−2257.

(13) Tran, C. D.; Duri, S.; Delneri, A.; Franko, M. Chitosan-cellulose composite materials: preparation, characterization and application for removal of microcystin. *J. Hazard. Mater.* **2013**, *252*, 355−366.

(14) Harkins, A. L.; Duri, S.; Kloth, L. C.; Tran, C. D. Chitosan−cellulose composite for wound dressing material. Part 2. Antimicrobial activity, blood absorption ability, and biocompatibility. *J. Biomed. Mater. Res., Part B* **2014**, *102*, 1199−1206.

(15) Pelton, J. T.; McLean, L. R. Spectroscopic Methods for Analysis of Protein Secondary Structure. *Anal. Biochem.* **2000**, *277*, 167−176.

(16) Kuroda, R.; Honma, T. CD spectra of solid-state samples. *Chirality* **2000**, *12*, 269−277.

(17) Kuroda, R.; Harada, T. Solid State Chiroptical Spectroscopy: Principles and Applications. In *Comprehensive Chiroptical Spectroscopy. Vol 1: Instrumentation, and Theoretical Simulations*; Berova, N.; Polavarapu, P. L.; Nakanishi, K.; Woody, R. W., Eds.; John Wiley: Hoboken, NJ, 2012; pp 91−113.

(18) Oldfield, E. Chemical shifts and three-dimensional protein structures. *J. Biomol. NMR* **1995**, *5*, 217−225.

(19) Wishart, D. S.; Sykes, B. D. the 13C chemical shift index: a simple method for the identification of protein secondary structure using 13C chemical shift data. *J. Biomol. NMR* **1994**, *4*, 171−180.

(20) Dousseau, F.; Pezolet, M. Determination of the secondary structure content of proteins in aqueous solutions from their amide I and amide II infrared bands. Comparison between classical and partial least-squares methods. *Biochemistry* **1990**, *29*, 8771−8779.

(21) Arrondo, J. L. R.; Muga, A.; Castresana, J.; Goñi, F. M. Quantitative studies of the structure of proteins in solution by Fourier-transform infrared spectroscopy. *Prog. Biophys. Mol. Biol.* **1993**, *59*, 23−56.

(22) Tamm, L. K.; Tatulian, S. A. Infrared spectroscopy of proteins and peptides in lipid bilayers. *Q. Rev. Biophys.* **1997**, *30*, 365−429.

DOI: 10.1021/acssuschemeng.6b00084
ACS Sustainable Chem. Eng. 2016, 4, 1850−1861

(23) Dong, A.; Huang, P.; Caughey, W. S. Protein secondary structures in water from second-derivative amide I infrared spectra. *Biochemistry* **1990**, *29*, 3303−3308.
(24) Duri, S.; Majoni, S.; Hossenlopp, J. M.; Tran, C. D. Determination of Chemical Homogeneity of Fire Retardant Polymeric Nanocomposite Materials by Near-infrared Multispectral Imaging Microscopy. *Anal. Lett.* **2010**, *43*, 1780−1789.
(25) Cardamone, J. M. Investigating the microstructure of keratin extracted from wool: Peptide sequence (MALDI-TOF/TOF) and protein conformation (FTIR). *J. Mol. Struct.* **2010**, *969*, 97−105.
(26) Pelton, J. T.; McLean, L. R. Spectroscopic methods for analysis of protein secondary structure. *Anal. Biochem.* **2000**, *277*, 167−176.
(27) Wold, S.; Sjöström, M.; Eriksson, L. PLS-regression: a basic tool of chemometrics. *Chemom. Intell. Lab. Syst.* **2001**, *58*, 109−130.
(28) Arrondo, J. L. R.; Muga, A.; Castresana, J.; Goñi, F. M. Quantitative studies of the structure of proteins in solution by Fourier-transform infrared spectroscopy. *Prog. Biophys. Mol. Biol.* **1993**, *59*, 23−56.
(29) Tamm, L. K.; Tatulian, S. A. Infrared spectroscopy of proteins and peptides in lipid bilayers. *Q. Rev. Biophys.* **1997**, *30*, 365−429.
(30) Dong, A.; Huang, P.; Caughey, W. S. Protein secondary structures in water from second-derivative amide I infrared spectra. *Biochemistry* **1990**, *29*, 3303−3308.
(31) Kumosinski, T. F.; Unruh, J. J. Quantitation of the global secondary structure of globular proteins by FTIR spectroscopy: comparison with X-ray crystallographic structure. *Talanta* **1996**, *43*, 199−219.
(32) Westad, F.; Schmidt, A.; Kermit, M. Incorporating chemical band-assignment in near infrared spectroscopy regression models. *J. Near Infrared Spectrosc.* **2008**, *16*, 265−273.
(33) Westad, F.; Martens, H. Variable selection in near infrared spectroscopy based on significance testing in partial least squares regression. *J. Near Infrared Spectrosc.* **2000**, *8*, 117−124.
(34) Anderssen, E.; Dyrstad, K.; Westad, F.; Martens, H. Reducing over-optimizm in variable selection by cross-model validation. *Chemom. Intell. Lab. Syst.* **2006**, *84*, 69−74.
(35) Westad, F.; Afseth, N. K.; Bro, R. Finding relevant spectral regions between spectroscopic techniques by use of cross model validation and partial least squares regression. *Anal. Chim. Acta* **2007**, *595*, 323−327.
(36) Bernstein, F. C.; Koetzle, T. F.; Williams, G. J. B.; Meyer, E. F., Jr; Brice, M. D.; Rodgers, J. R.; Kennard, O.; Shimanouchi, T.; Tasumi, M. The Protein Data Bank: a computer-based archival file for macromolecular structures. *Arch. Biochem. Biophys.* **1978**, *185*, 584−591.
(37) Kabsch, W.; Sander, C. Dictionary of protein secondary structure: pattern recognition of hydrogen-bonded and geometrical features. *Biopolymers* **1983**, *22*, 2577−2637.
(38) Li, R.; Wang, D. Preparation of regenerated wool keratin films from wool keratin−ionic liquid solutions. *J. Appl. Polym. Sci.* **2013**, *127*, 2648−2653.
(39) Peplow, P. V.; Roddick-lanzilotta, A. D. Orthopaedic materials derived from keratin. U.S. Patent 20,050,232,963, October 20, 2005.
(40) Sowa, M. G.; Wang, J.; Schultz, C. P.; Ahmed, M. K.; Mantsch, H. H. Infrared spectroscopic investigation of *in vivo* and *ex vivo* human nails. *Vib. Spectrosc.* **1995**, *10*, 49−56.
(41) Karaman, İ.; Qannari, E. M.; Martens, H.; Hedemann, M. S.; Knudsen, K. E. B.; Kohler, A. Comparison of Sparse and Jack-knife partial least squares regression methods for variable selection. *Chemom. Intell. Lab. Syst.* **2013**, *122*, 65−77.
(42) Navea, S.; Tauler, R.; de Juan, A. Application of the local regression method interval partial least-squares to the elucidation of protein secondary structure. *Anal. Biochem.* **2005**, *336*, 231−242.
(43) Dickerson, M. B.; Sierra, A. A.; Bedford, N. M.; Lyon, W. J.; Gruner, W. E.; Mirau, P. A.; Naik, R. R. Keratin-based antimicrobial textiles, films, and nanofibers. *J. Mater. Chem. B* **2013**, *1*, 5505−5514.
(44) Aluigi, A.; Zoccola, M.; Vineis, C.; Tonin, C.; Ferrero, F.; Canetti, M. Study on the structure and properties of wool keratin regenerated from formic acid. *Int. J. Biol. Macromol.* **2007**, *41*, 266−273.
(45) Cardamone, J. M. Investigating the microstructure of keratin extracted from wool: Peptide sequence (MALDI-TOF/TOF) and protein conformation (FTIR). *J. Mol. Struct.* **2010**, *969* (1), 97−105.
(46) Greve, T. M.; Andersen, K. B.; Nielsen, O. F. Penetration mechanism of dimethyl sulfoxide in humand and pig ear skin: An ATR-FTIR and near-FT Raman Spectroscopic *in vivo* and *in vitro* study. *Spectroscopy* **2008**, *22*, 405−417.
(47) Cilurzo, F.; Selmin, F.; Aluigi, A.; Bellosta, S. Regenerated keratin proteins as potential biomaterial for drug delivery. *Polym. Adv. Technol.* **2013**, *24*, 1025−1028.
(48) Yoshimizu, H.; Ando, I. Conformational characterization of wool keratin and S-(carboxymethyl) kerateine in the solid state by carbon-13 CP/MAS NMR spectroscopy. *Macromolecules* **1990**, *23*, 2908−2912.
(49) Dickerson, M. B.; Sierra, A. A.; Bedford, N. M.; Lyon, W. J.; Gruner, W. E.; Mirau, P. A.; Naik, R. R. Keratin-based antimicrobial textiles, films, and nanofibers. *J. Mater. Chem. B* **2013**, *1*, 5505−5514.
(50) Tanabe, T.; Okitsu, N.; Tachibana, A.; Yamauchi, K. Preparation and characterization of keratin−chitosan composite film. *Biomaterials* **2002**, *23*, 817−825.
(51) Hameed, N.; Guo, Q. Blend films of natural wool and cellulose prepared from an ionic liquid. *Cellulose* **2010**, *17*, 803−813.
(52) Persson, A. M.; Sokolowski, A.; Pettersson, C. Correlation of *in vitro* dissolution rate and apparent solubility in buffered media using a miniaturized rotating disk equipment: Part l. Comparison with a traditional USP rotating disk apparatus. *Drug Discovery Ther.* **2009**, *3*, 104−113.

DOI: 10.1021/acssuschemeng.6b00084
ACS Sustainable Chem. Eng. 2016, 4, 1850−1861